International Journal of Automotive Technology, Vol. 17, No. 3, pp. 447–456 (2016)
DOI 10.1007/s12239–016–0046–5

pISSN 1229–9138/ eISSN 1976–3832

COOPERATIVE CONTROL OF THE MOTOR AND THE ELECTRIC BOOSTER BRAKE TO IMPROVE THE STABILITY OF AN IN-WHEEL ELECTRIC VEHICLE

S. KO, C. SONG and H. KIM*

Department of Mechanical Engineering, Sungkyunkwan University, Gyeonggi 16419, Korea

(Received 25 March 2015; Revised 16 October 2015; Accepted 21 October 2015)

ABSTRACT–A cooperative control algorithm for an in-wheel motor and an electric booster brake is proposed to improve the stability of an in-wheel electric vehicle. The in-wheel system was modeled by dividing it into motor and mechanical parts, and the electric booster brake was modeled through tests. In addition, the response characteristics of the in-wheel system and the electric booster brake were compared through a frequency response analysis. In the cooperative control, the road friction coefficient was estimated using the wheel speed, motor torque, and braking torque of each wheel, and the torque limit of the wheel to the road was determined using the estimated road friction coefficient. Based on the estimated road friction coefficient and torque limit, a cooperative algorithm to control the motor and the electric booster brake was proposed to improve the stability of the in-wheel electric vehicle. The performance of the proposed cooperative control algorithm was evaluated through a hardware-in-the-loop simulation (HILS). Furthermore, to verify the performance of the proposed cooperative control algorithm, a test environment was constructed for the anti-lock braking system (ABS) hydraulic module hardware, and the performance of the cooperative control algorithm was compared with that of the ABS by means of a HILS test.

KEY WORDS : Cooperative control, In-wheel, Electric booster brake, Vehicle stability, Slip control

1. INTRODUCTION

In an in-wheel electric vehicle (an electric vehicle with a motor installed in each wheel), each motor transmits its power directly to a wheel. The in-wheel electric vehicle, through independent control of the in-wheel motor at each wheel, offers advantages in the implementation of active safety systems such as traction control, anti-lock braking, and electronic stability control (Dong *et al*., 2012). Also, the in-wheel system has been reported to reduce by 10 ~ 30 % the time delay in the yaw speed change at a low vehicle speed, compared to a conventional vehicle, through independent controls such as the quick and accurate generation of left and right wheel torques in opposite directions (Sakai *et al*., 1999; Jacobsen, 2002).

Various studies have been conducted to improve the stability of in-wheel electric vehicles. Because the torque of each wheel of an in-wheel electric vehicle can be easily measured based on the current of the in-wheel motors, a simple driving force observer can be designed, and the driving and braking forces between a tire and the road surface can be easily estimated in real time (Hori *et al*., 2004). Also, studies have been conducted on wheel-slip control using the back electromotive force of the motor (Liu *et al*., 2005), on torque control of the in-wheel motor based on estimation of the road friction coefficient (Ko *et al*., 2015b), on in-wheel motor torque control based on sliding-mode control (Kim *et al*., 2011), on improvement of vehicle stability by integrating in-wheel motor control with slip control, yaw rate control, and velocity control (Ko *et al*., 2013a), on lateral stability control based on sideslip angle estimation using lateral tire force sensors (Nam *et al*., 2012), and on the optimal torque distribution of four in-wheel motors for vehicle stability (Chen and Kuo, 2014). However, the in-wheel electric vehicle cannot achieve the desired braking performance for quick braking or high-speed braking on high-friction roads where the braking force of the in-wheel motor is insufficient due to some limitations such as with the motor characteristics and the battery's state of charge (Ko *et al*., 2013b).

Therefore, an in-wheel electric vehicle must have a friction brake system that enables active cooperative control, together with the in-wheel motor, according to the braking demand of the driver and the driving state (Walker *et al*., 2002). Brake-by-wire systems have been used in friction brake systems such as electronic hydraulic brakes (EHB) or electric actuators. Various EHBs have been developed, such as an electronically controlled brake system that uses an oil pump and a hydraulic control unit (Soga *et al*., 2002; Park *et al*., 2009), a smart booster system that uses an electrical booster (Fujiki *et al*., 2011; Yeo *et al*., 2011), and a ball screw drive module (Kawaguchi and

**Corresponding author.* e-mail: hskim@me.skku.ac.kr

Kazuno, 2013). Also, many electronic brake systems have been developed such as the electronic mechanical brake (EMB) and the electronic wedge-type brake (EWB).

Using the EHB and the electric actuator, various studies have been conducted to increase energy recovery through cooperative control of the motor and the friction brake, including cooperative control for parallel hybrid electric vehicles (HEVs) with electric booster brakes (Kim *et al*., 2011), cooperative control using a front EWB and a rear hydraulic brake for automatic-transmission-based HEVs (Ko *et al*., 2015a), and cooperative control using an EMB and an EWB for HEVs (Ko *et al*., 2011, 2012). However, most studies on the cooperative control for the regenerative braking and the friction braking have been performed when driving on the high friction coefficient road where the demanded braking force is smaller than the transmittable force between the tire and road.

In this study, a cooperative control algorithm is proposed for the in-wheel motor and the friction brake to improve the stability when the demanded deceleration exceeds the available deceleration for the given road surface. For slip control, a cooperative control algorithm for slips is proposed that considers the response characteristics of an in-wheel system and an electric booster brake system. The performance of the proposed cooperative control algorithm was evaluated by means of hardware-in-the-loop simulation (HILS) and compared with the performance of the ABS module.

2. MODELING AND ANALYSIS OF THE IN-WHEEL SYSTEM AND THE ELECTRIC BOOSTER BRAKE

To develop the cooperative control algorithm, dynamic models of the in-wheel system and the electric booster were developed.

2.1. In-wheel System

The structure of the in-wheel system investigated in this study is illustrated schematically in Figure 1. The target in-wheel system consisted of an in-wheel motor, reduction gear, bearing, axle, disk, and caliper. The in-wheel motor specifications are that the motor power is 16 kW and the maximum torque is 125 Nm.

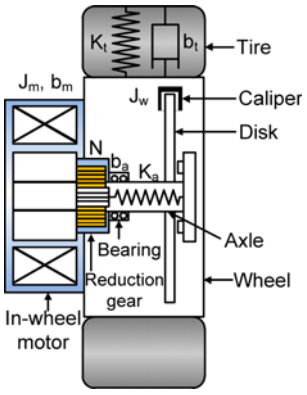

Figure 1. Structure of the in-wheel system.

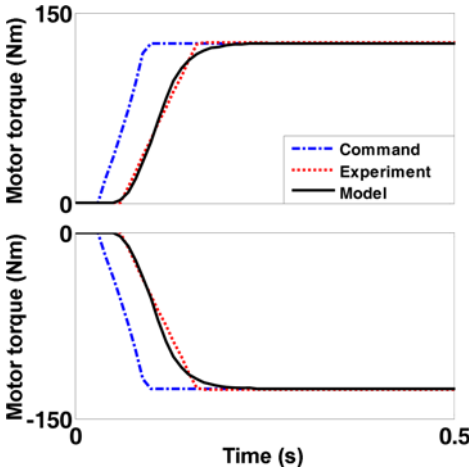

Figure 2. Experimental validation of the motor model.

2.1.1. In-wheel motor model

The torque dynamics of the in-wheel motor was modeled as a first-order system as follows;

$$T_m = \frac{1}{\tau s + 1} e^{-\tau_d s} T_{cmd} = G_{motor} T_{cmd} \quad (1)$$

where T_m is the in-wheel motor torque, τ is the time constant, τ_d is the time delay, G_{motor} is the transfer function of the in-wheel motor, and T_{cmd} is the motor torque command. The in-wheel motor model was validated by using the motor test results (Figure 2). For the simulation and test, commands were given to apply maximum torque in the (a) positive and (b) negative directions. In the motor model, the time constants $\tau = 0.01$ and $\tau_d = 0.01$ were used. From Figure 2, it was found that the motor model showed a good agreement with experimental results.

2.1.2. In-wheel mechanical system model

The in-wheel mechanical system was modeled through a Bondgraph (Figure 3).

From the Bondgraph model in Figure 3, the following state equations were derived;

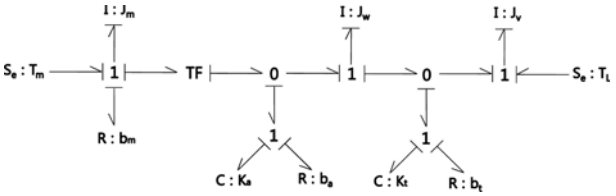

Figure 3. Bondgraph model of the in-wheel mechanical system.

$$\frac{d}{dt}\begin{bmatrix} h_m \\ \theta_a \\ h_w \\ \theta_t \\ h_t \end{bmatrix} = \begin{bmatrix} -\frac{b_m}{J_m}+\frac{b_a}{J_m N^2} & \frac{K_a}{N} & -\frac{b_a}{J_w N} & 0 & 0 \\ \frac{1}{J_m N} & 0 & \frac{1}{J_w} & 0 & 0 \\ \frac{b_a}{J_m N} & K_a & -\frac{b_a}{J_w}+\frac{b_t}{J_w} & -K_t & -\frac{b_t}{J_v} \\ 0 & 0 & \frac{1}{J_w} & 0 & -\frac{1}{J_v} \\ 0 & 0 & \frac{b_t}{J_w} & K_{tire} & -\frac{b_t}{J_v} \end{bmatrix} \begin{bmatrix} h_m \\ \theta_a \\ h_w \\ \theta_t \\ h_t \end{bmatrix} + \begin{bmatrix} T_m \\ 0 \\ 0 \\ 0 \\ T_L \end{bmatrix} = Ax + Bu \quad (2)$$

where h is the angular momentum, T is the torque, b is the damping ratio, J is the inertia, N is the gear ratio, K is the stiffness, and θ is the angle; subscript m refers to the motor, a to the axle, w to the wheel, t to the tire, v to the vehicle, and L to the load. In the in-wheel mechanical system model, the effects of the reduction gear stiffness, the backlash and the efficiency are neglected.

The torque from the motor that acts on the wheel can be determined as follows;

$$T_w = \begin{bmatrix} 0 & 0 & 0 & K_t & 0 \end{bmatrix} \begin{bmatrix} h_m \\ \theta_a \\ h_w \\ \theta_t \\ h_t \end{bmatrix} = Cx \quad (3)$$

From Equations (2) and (3), the transfer function of the in-wheel mechanical system G_{mech} of the torque T_w that acts on the wheel for the given motor torque T_m is expressed as follows;

$$G_{mech} = \frac{T_w}{T_m} = C(SI - A)^{-1}B \quad (4)$$

2.1.3. Frequency response of the in-wheel system

The transfer function of the in-wheel mechanical system $G_{in\text{-}wheel}$ of the torque T_w for the wheel the given motor torque command T_{cmd} is expressed as follows;

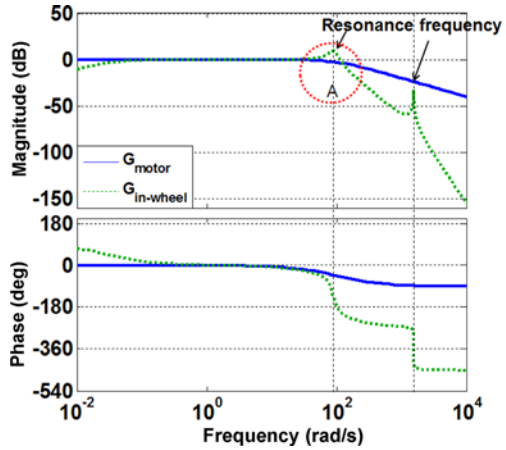

Figure 4. Frequency response of the in-wheel motor and the in-wheel system.

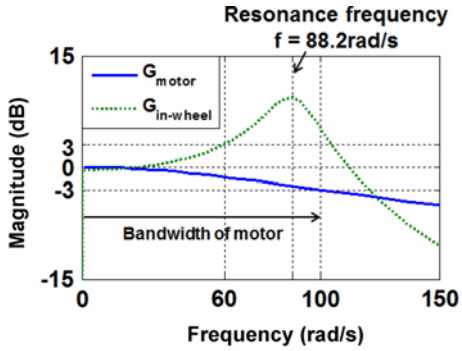

Figure 5. Frequency response of the in-wheel motor and the in-wheel system in Region A.

$$G_{in\text{-}wheel} = \frac{T_w}{T_{cmd}} = G_{motor} G_{mech} \quad (5)$$

Figure 4 shows the frequency response of the in-wheel motor and the in-wheel system. The in-wheel system had the resonance frequencies of f = 88.2 rad/s and 1,530 rad/s, which were not observed for the in-wheel motor. To compare the response characteristics of the system, Region A of Figure 4 was magnified and is shown in Figure 5.

Even though the bandwidth of the in-wheel motor was 100 rad/s, for the in-wheel system with an in-wheel motor and a mechanical system, the magnitude increased to over 3 dB when the frequency exceeded 60 rad/s. Because of the resonance at 88.2 rad/s, the system must be controlled at a lower frequency.

2.2. Electric Booster Brake

For cooperative control with the in-wheel system, the electric booster brake was used as a friction brake.

Figure 6 shows the structure of the electric booster brake, which consisted of the actuator, the screw, the master cylinder, and conventional brake parts including the hydraulic pipe line and the calipers.

Figure 7 shows the electric booster brake bench tester. The frequency response of the electric booster brake was

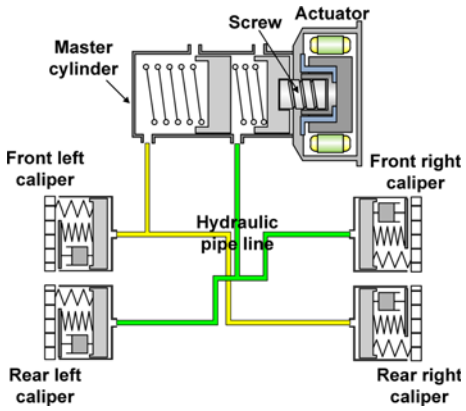

Figure 6. Structure of the electric booster brake.

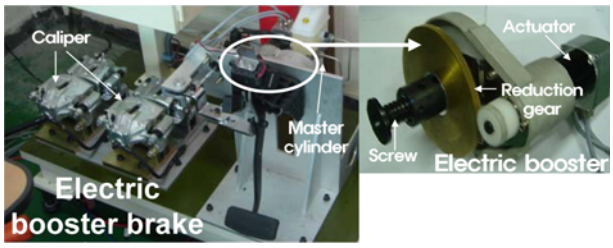

Figure 7. Electric booster brake bench tester.

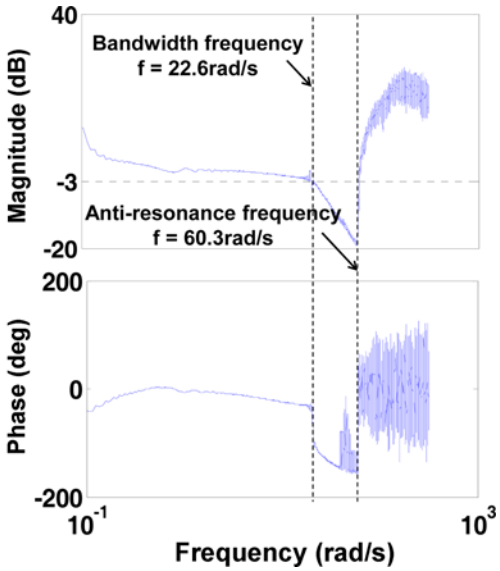

Figure 8. Frequency response of the electric booster brake measured using the bench tester.

obtained using this tester. It was found that the bandwidth frequency of the electric booster brake system was 22.6 rad/s, which is smaller than that of the in-wheel system.

The output pressure Pout of the electric booster was transformed to braking torque as follows;

$$T_{fb} = 2\mu_{disk} P_{out} A_{cyl} r_{eff} \tag{6}$$

where μ_{disk} is the friction coefficient of the disk, A_{cyl} is the area of the caliper cylinder, and r_{eff} is the effective radius.

3. COOPERATIVE CONTROL OF THE IN-WHEEL MOTOR AND THE ELECTRIC BOOSTER BRAKE

Using the in-wheel and electric booster brake models, a cooperative control algorithm was developed. This algorithm included estimation of the road friction coefficient and setting of the torque limit, and control of the electric booster brake and the motor torque.

3.1. Road Friction Coefficient Estimation and Torque Limit Determination

Many road friction coefficient estimation methods have been reported, including the use of a linear slope of a longitudinal force according to the slip ratio by friction coefficient (Nakao *et al*., 2002); the use of a nonlinear tire model (Wang *et al*., 2004); consideration of weight transfer with a full car model (Lee *et al*., 2010); the use of a Kalman filter based on the wheel velocity, acceleration sensor, and GPS information (Rajamani *et al*., 2010); real-time estimation of the road friction coefficient of each wheel using the engine torque, brake torque, GPS measurements, and accelerometer measurements (Rajamani *et al*., 2012); and estimation methods based on the estimated longitudinal force through the design of a PI observer (Ko *et al*., 2015b). In the present study, a road friction coefficient estimation method was developed by modifying an existing method (Ko *et al*., 2015b).

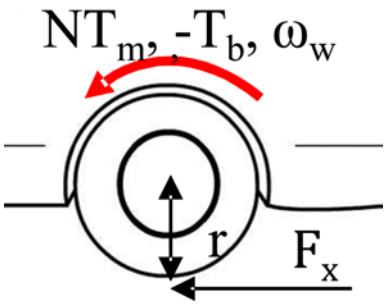

Figure 9. Wheel dynamics.

The wheel dynamic equation can be derived from Figure 9 as follows;

$$J_w \dot{\omega}_w = NT_m - T_b - rF_x \tag{7}$$

The estimator of the longitudinal force was designed as a PI observer as follows (Ko *et al*., 2015b);

$$\hat{F}_{xi} = -l_0(\omega_{wi} - \hat{\omega}_{wi}) - \int l_1(\omega_{wi} - \hat{\omega}_{wi})d\tau \tag{8}$$

where $\hat{\omega}_{wi}$ is the estimated angular velocity of the wheels, $\hat{F}_{xi}$ is the estimated longitudinal force on the tire, and l_0 and l_1 are the PI observer gains. Using the estimated $\hat{\omega}_{wi}$, Equation (8) can be represented as follows;

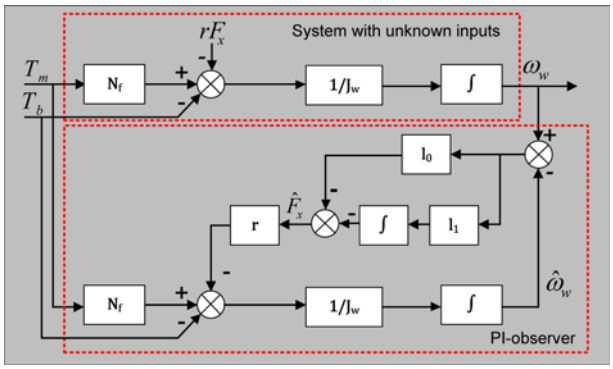

Figure 10. Block diagram of the longitudinal force PI observer.

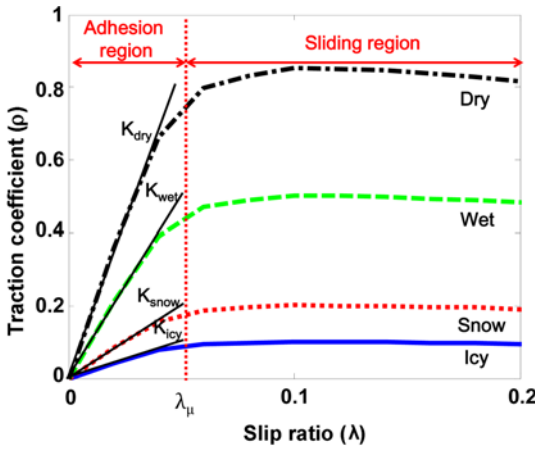

Figure 11. Nonlinear tire model (Traction coefficient versus slip ratio).

$$J_w\dot{\hat{\omega}}_w = N_f T_m - T_b - r\hat{F}_x \tag{9}$$

Figure 10 shows a block diagram of the longitudinal force PI observer.

Figure 11 shows the nonlinear tire model. The tire traction coefficient changes according to the slip ratio for various road surfaces. It is seen that the traction coefficient increases when the slip ratio λ ranges between 0 and λ_μ (adhesion region) and remains almost constant when $\lambda > \lambda_\mu$ (sliding region). In the sliding region, the road friction coefficient can be estimated using the longitudinal force that acts on the tire, through the following Equation (6);

$$\mu_{est} = \rho = \frac{\hat{F}_x}{F_z} \quad for\ \lambda_i \geq \lambda_\mu\ (sliding\ region) \tag{10}$$

where μ_{est} is the estimated road friction coefficient, ρ is the traction coefficient, and F_z is the normal force. In this study, a road coefficient estimation method is proposed that uses the longitudinal force on the tire, which is estimated based on the linear increase of the traction coefficient ρ according to increases in the slip ratio in the adhesion region. The traction coefficient ρ was linearized with respect to the slip ratio by the following equation;

$$\rho = \frac{\hat{F}_x}{F_z} = K_{road}\lambda \quad for\ \lambda_i < \lambda_\mu\ (adhesion\ region) \tag{11}$$

where K_{road} is the slip slope, which depends on the road surface conditions. K_{road} can be estimated based on the longitudinal force on the tire, the slip ratio, and the normal force in the adhesion region as follows;

$$K_{road} = \frac{\hat{F}_x}{\lambda F_z} \tag{12}$$

The estimated K_{road} is changed to the road friction coefficient using the nonlinear tire model in Figure 11.

Using this estimated road friction coefficient, the torque limit T_{limit} on the wheel can be obtained using the following equation;

$$T_{limit} = r\mu_{est}F_z \tag{13}$$

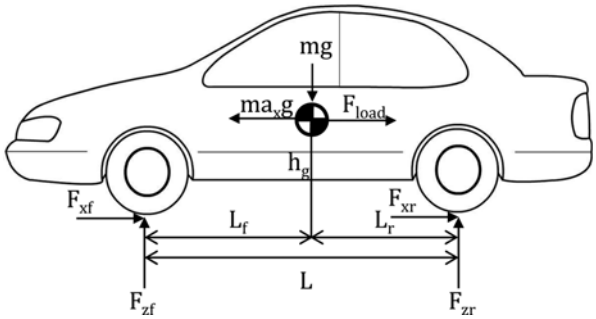

Figure 12. Forces that act on the vehicle during braking.

3.2. Electric Booster Brake Control

The torque distribution of the in-wheel system and the friction brake is determined by the pressure of the electric booster brake and the in-wheel motor torque of each wheel. The electric booster brake generates friction brake torques at a constant ratio to the front and rear wheels, and the friction brake torque must be examined first at the vehicle level.

Figure 12 illustrates the forces that act on the vehicle during braking. The normal forces F_{zf} and F_{zr}, which act vertically on the front and rear wheels, are computed as follows;

$$F_{zf} = \frac{mg}{L}(L_r + h_g a_x) - \frac{h_g}{L}F_{load} \tag{14}$$

$$F_{zr} = \frac{mg}{L}(L_f - h_g a_x) + \frac{h_g}{L}F_{load} \tag{15}$$

where m is the vehicle's mass, g is the gravitational acceleration, L is the distance between the front and rear wheels, L_f is the distance between the center of mass and the front wheel, L_r is the distance between the center of mass and the rear wheel, h_g is the horizontal distance between the road surface and the center of mass, a_x is the coefficient of deceleration (expressed in terms of g), and F_{load} is the road load.

If the braking force is greater than the friction force between the tire and the road, excessive slip may occur, which will lead to wheel locking. To prevent wheel locking, the braking forces F_{xf} and F_{xr} that act on the front and rear wheels must satisfy the following equations;

$$F_{xf} \leq \mu F_{zf} = \frac{\mu mg}{L}(L_r + h_g a_x) - \frac{\mu h_g}{L}F_{load} \tag{16}$$

$$F_{xr} \leq \mu F_{zr} = \frac{\mu mg}{L}(L_f - h_g a_x) + \frac{\mu h_g}{L}F_{load} \tag{17}$$

To further prevent wheel locking, the total braking force must satisfy the following equation;

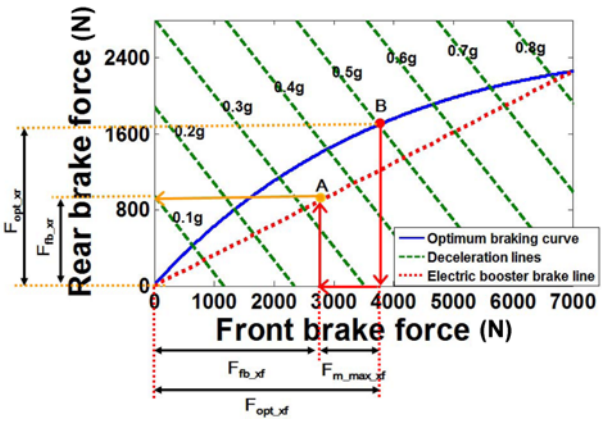

Figure 13. Braking force distribution.

$$F_{xf} + F_{xr} = ma_x g - F_{load} \le \mu(F_{zf} + F_{zr}) = \mu mg \tag{18}$$

Equation (18) can be expressed as follows;

$$a_x \le \mu + \frac{F_{load}}{mg} \tag{19}$$

In other words, the maximum deceleration of the vehicle can be determined if the road friction coefficient μ and the ratio F_{load}/mg are both known. Because F_{load} is negligible compared to the μmg term, if the maximum deceleration is assumed to be equal to the road friction coefficient (Limpert, 1992), in Equations (16) ~ (18), the braking forces F_{xf} and F_{xr} that act on the front and rear wheels can be correlated as follows;

$$F_{xr} = mg\sqrt{(\frac{L_r}{2h_g})^2 + \frac{L}{mgh}F_{xf}} - \frac{mgL_r}{2h} - F_{xf} \tag{20}$$

Equation (20) is plotted in Figure 13 as the optimum braking curve.

In general, the cooperative controls have been carried out to distribute the regenerative braking force and the friction braking force in terms of the energy recovery when the demanded braking deceleration is smaller than the maximum deceleration for the given road surface (Kim *et al*., 2011; Ko *et al*., 2015b). In this study, a cooperative control algorithm was proposed when the demanded braking deceleration exceeds the maximum deceleration for the given road surface.

Figure 13 shows the braking force distribution in the cooperative control algorithm proposed in this study. In the figure, deceleration lines indicate the required front and rear wheel braking forces corresponding to the demanded deceleration. Since it can be assumed that the maximum braking deceleration is equal to the road friction coefficient from Equation (19) (Limpert, 1992), the maximum deceleration can be determined from the estimated road friction coefficient. For the given estimated road friction coefficient, the front and rear braking forces are determined from the optimum braking curve. For example, when the estimated road friction coefficient is $\mu_{est} = 0.5$, the front and rear wheel braking forces F_{opt_xf} and F_{opt_xr} are determined at the point B from the optimum braking curve in response to the maximum deceleration of 0.5 g. When the front maximum motor regenerative force (torque) is $F_{m\_max\_xf}$ for the given motor characteristic, the front friction braking force is obtained by subtracting $F_{m\_max\_xf}$ from F_{opt_xf} as follows;

$$F_{fb\_xf} = F_{opt\_xf} - F_{m\_max\_xf} \tag{21}$$

Then the rear friction braking force F_{fb_xr} is determined at the point B from the electric booster brake line for F_{fb_xf}. In this study, the electric booster brake line is designed to be linear, which is below the optimum braking curve by considering the geometric constraints of the brake system such as the master cylinder, the piston area, etc. The reason why the front friction braking force F_{fb_xf} is determined first rather than the rear braking force is that the front braking forces are larger than the rear braking forces in the target in-wheel electric vehicle.

From Equations (6) and (21), the command pressure P_{fb_c} of the electric booster brake can be expressed as follows;

$$P_{fb\_c} = \frac{F_{opt\_xf} - \frac{T_{m\_max\_f}}{r}}{2\mu_{disk}A_{cyl\_f}} \tag{22}$$

where $T_{m\_max\_f}$ is the front maximum motor regenerative torque.

3.3. Motor Torque Control

For motor torque control, the motor torque command T_{m_c} is determined using the previously determined torque limit and friction braking force.

$$T_{m\_c} = T_{limit} - T_{fb} = T_{limit} - 2\mu_{disk}A_{cyl}r_{eff}P_{fb\_c} \tag{23}$$

The motor torque prevents slipping of the vehicle by generating a torque close to the optimum braking curve. If T_{fb} is 0, braking only with the motor torque is possible, so the motor torque is determined as the torque limit (T_{limit}).

3.4. Block Diagram of the Cooperative Control

Figure 14 shows the block diagram of the proposed cooperative control. The co-operative control consists of 3 parts: A. Road friction coefficient estimation and torque limit decision, B. Electric booster brake control and C. Motor torque control. In A, the longitudinal force that acts on the tire is estimated and used to estimate the road friction coefficient. The estimated road friction coefficient is used to obtain the T_{limit} of each wheel.

In B, the maximum deceleration is determined based on the estimated road friction coefficient, and the command pressure of the electric booster brake is determined based on the maximum deceleration. In C, the in-wheel motor torque command T_{m_c} of each wheel is obtained using the previously determined T_{limit} and command pressure P_{fb_c}.

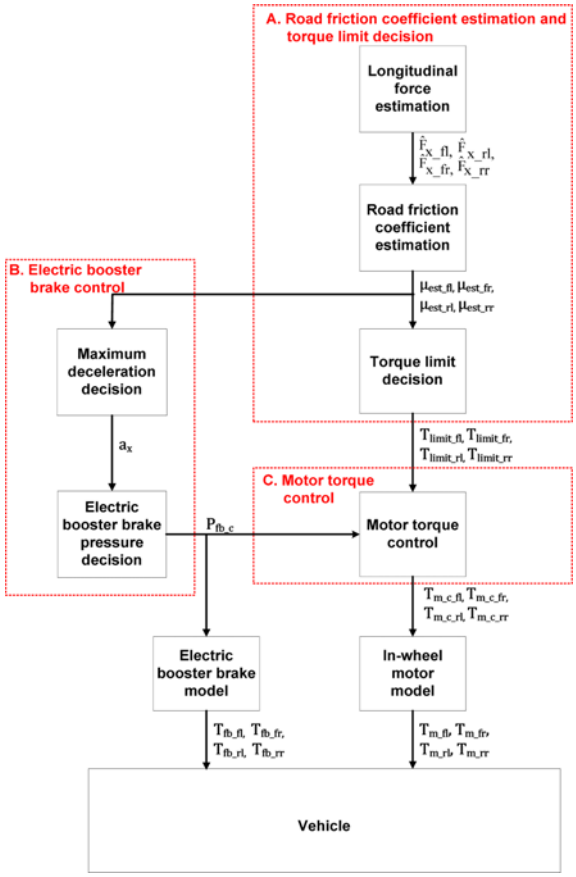

Figure 14. Block diagram of the cooperative control.

The final command is converted to the torque of each wheel through the in-wheel motor model and the electric booster brake model, and these torques are input to the vehicle.

4. HARDWARE-IN-THE-LOOP SIMULATION (HILS)

To verify the performance of the proposed cooperative control algorithm, HILS simulation was performed. Table 1 shows the vehicle specifications used in the HILS.

Figure 15 illustrates the schematic diagram of the HILS system. The system's software consisted of a controller and an in-wheel system model developed based on MATLAB, and a vehicle model developed based on CarSim RT. The hardware consisted of an electric booster brake, a control box, and a dSPACE ds1005/ds2201 board. The dSPACE board also performed real-time simulation together with CarSim RT. The MATLAB simulator received the electric booster brake pressure Pfb_sensor measured by the sensor, and input the motor torque and the friction brake torque of each wheel to the CarSim RT vehicle model. The CarSim RT vehicle model input to the MATLAB simulator the vehicle states such as the vehicle velocity, wheel speed, deceleration, etc.

Table 1. Vehicle specifications.

Parameters		
Vehicle	Sprung mass	1,200 kg
	Distance between the center of gravity of the sprung mass and the front wheel centerline	1,103 mm
	Distance between the center of gravity of the sprung mass and the rear wheel centerline	1,244 mm
	Distance between the front and rear wheel centerlines	2,347 mm
	Height of the vehicle above the center of gravity	540 mm
	Track width	1,595 mm
	Tire effective rolling radius	273.6 mm
	Frontal area	1.9 m^2
In-wheel motor	Power	16 kW
	Maximum torque	123.2 N·m
	Maximum speed	5,000 rpm
	Reduction gear ratio	4
Battery	Nominal voltage	270 V
	Capacity	1.2 A·h

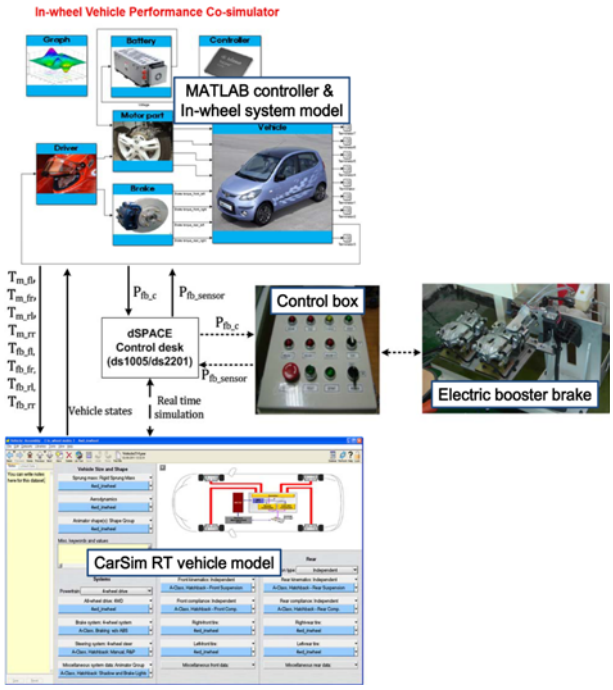

Figure 15. Schematic of the HILS system.

Figure 16 shows the electric booster brake hardware system. The electric booster brake consisted of the electric

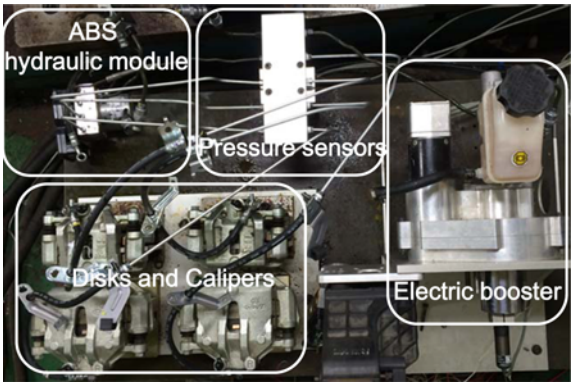

Figure 16. Electric booster brake hardware system.

booster, pressure sensors, disks, and calipers. In addition, the ABS hydraulic module was used to compare the performance of the ABS with that of the proposed cooperative control algorithm of the in-wheel motors and electric booster brake.

The HILS was performed for the cases of (1) ABS braking and (2) cooperative control of the in-wheel motor and the electric booster brake, both on a wet road with the road friction coefficient $\mu = 0.5$ and at 100 km/h; then, the braking performances of the two systems were compared.

4.1. ABS

Figure 17 shows the HILS results for the ABS braking. When the vehicle was simulated to brake on a wet road with the road friction coefficient $\mu = 0.5$, the velocity determined by multiplying the wheel speed by the wheel radius repeatedly decreased and increased (a and b) according to the slip ratio (c). This is because the ABS hydraulic module reduces the pressure when the slip ratio rises, and increase the pressure when the slip ratio falls. Therefore, the front and rear wheel pressures P_{fb_f} and P_{fb_r} were reduced in the periods when the slip ratio rose (c and d). Also, the friction brake torque repeatedly decreased and increased in response to changes in the front and rear wheel pressures (e). The slip ratio was 20 % ~ 30 % in the initial braking stage and rose to 90 % as the vehicle velocity decreased. The braking time was 6.8 s.

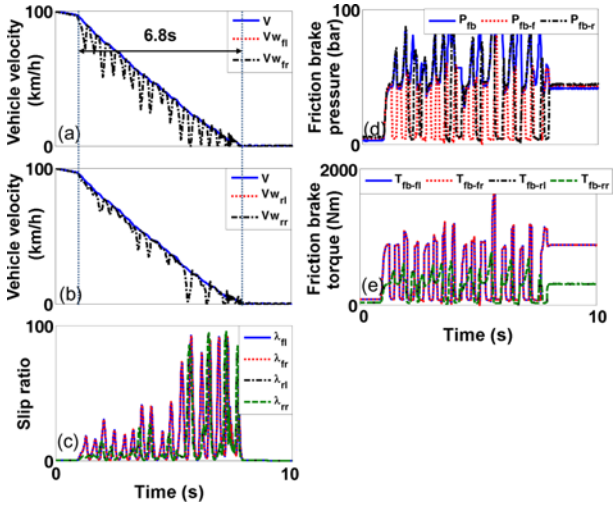

Figure 17. HILS results for ABS braking.

4.2. Cooperative Control

Figure 18 shows the HILS results for the cooperative control. The wheel velocity V_w during braking on the wet road fluctuated less under cooperative control than under ABS braking for both the front and rear wheels, and was almost identical to the vehicle velocity V (a and b). The slip ratio was less than 15 % for both the front and rear wheels (c). The estimated road friction coefficients of the front wheels, μ_{est_fl} and μ_{est_fr} were near 0.5 during early braking and increased to 0.65 as the vehicle velocity decreased, and μ_{est_rl} and μ_{est_rr} of the rear wheels were around 0.5 (d). The estimated road friction coefficient of the front wheels increased to 0.65 because in Equation (12), the slip ratio remains constant even when the braking force that acts on the wheels increases. In the cooperative control algorithm, the friction braking pressure (e) is determined based on the estimated road friction coefficient; and to apply this pressure, friction brake torque (f) is distributed to the front and rear wheels. The T_{limit} of the front wheels (g) is greater than that of the rear wheels because the normal force that acts on the front wheels during braking is greater than the force that acts on the rear wheels. The front and rear wheel motor torques are determined by subtracting the friction brake torque from the T_{limit}. The front wheel motor torque (h) is greater than the rear wheel motor torque. The braking time was 4.9 s, which was shorter than the 6.8 s braking time of the ABS braking.

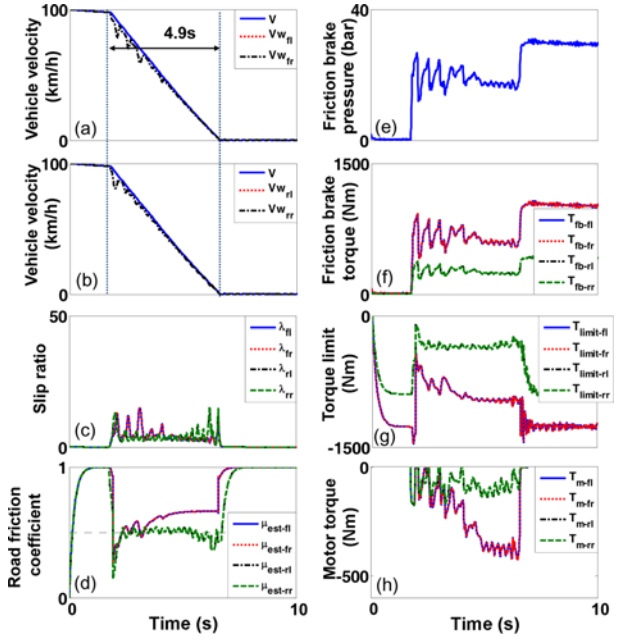

Figure 18. HILS results for the cooperative control.

The HILS results showed that the proposed cooperative control algorithm provided improved stability, with a lower slip ratio and faster braking time than the ABS hydraulic module.

5. CONCLUSION

A cooperative control algorithm for the in-wheel motor and the friction brake was proposed to improve the stability of an in-wheel electric vehicle incorporating an electric booster brake system. First, the in-wheel system was modeled by dividing it into motor and mechanical parts, and a transfer function was obtained for each system to investigate the frequency response. For the electric booster brake, a frequency response was obtained from the experiment, and the control bandwidth was analyzed by comparing it with the response characteristics of the in-wheel system. Furthermore, for cooperative control, a road friction coefficient estimation method was proposed using the wheel speed, motor torque, and braking torque of each wheel in both the adhesion and sliding regions. The cooperative control algorithm was proposed when the demanded braking deceleration exceeded the maximum deceleration. In the cooperative control, the maximum braking deceleration was determined from the estimated road friction coefficient. Using the maximum deceleration, the front friction braking force was obtained from the optimum braking curve considering the front maximum motor regenerative force (torque) and the rear friction braking force was obtained from the electric booster brake line. In addition, the torque limit of the wheel was determined using the estimated road friction coefficient. Using the torque limit and the friction brake torque, the motor torque was controlled to improve the stability. To verify the performance of the proposed cooperative control algorithm, a HILS system was constructed that consisted of the electric booster brake hardware, in-wheel system model, vehicle model, and controller software. The HILS results showed that the proposed cooperative control algorithm provided improved stability relative to a conventional ABS hydraulic module, with a lower slip ratio and a shorter braking time, which validated the performance of the proposed cooperative control algorithm.

ACKNOWLEDGEMENT–This work was supported by The Ministry of Trade, Industry and Energy and the Korea Institute for Advancement of Technology.

REFERENCES

Chen, B. and Kuo, C. (2014). Electronic stability control for electric vehicle with four in-wheel motors. *Int. J. Automotive Technology* **15**, **4**, 573–580.

Dong, Z., He, P., Han, C., Qi, Z., Deng, Z. and Qiu, H. (2012). The design of anti-slip control for in-wheel motor at the limited conditions in a four in-wheel-motor drive electric vehicle. *19th Int. Conf. Mechatronics and Machine Vision in Practice (M2VIP)*, 526–530.

Fujiki, N., Koike, Y., Itou, Y., Suzuki, G. and Goto, S. (2011). Development of an electrically-driven intelligent brake system for EV. *SAE Paper No*. 2011-39-7211.

Hori, Y. (2004). Future vehicle driven by electricity and control-research on four-wheel-motored "UOT electric march II". *IEEE Trans. Ind. Electron.* **51**, **5**, 954–962.

Jacobsen, B. (2002). Potential of electric wheel motors as new chassis actuators for vehicle maneuvering. *Proc. Inst. Mech. Eng., Part D: J. Automobile Eng.* **216**, **8**, 631–640.

Kawaguchi, H. and Kazuno, K. (2013). Ball screw drive module for electric hydraulic brake. *NTN Technical Review*, **81**, 36–39.

Kim, J., Ko, S., Lee, G., Yeo, H., Kim, P. and Kim, H. (2011). Development of co-operative control algorithm for parallel HEV with electric booster brake during regenerative braking. *IEEE Vehicle Power and Propulsion Conf*., 1–5.

Kim, J., Park, C., Hwang, S., Hori, Y. and Kim, H. (2011). Control algorithm for an independent motor-drive vehicle. *IEEE Trans. Vehicular Technology* **59**, **7**, 3213–3222.

Ko, J., Kim, J., Lee, G., Byun, S., Hyun, D. and Kim, H. (2011). Development of a co-operative control algorithm during regenerative braking for a fuel cell electric vehicle. *IEEE Vehicle Power and Propulsion Conf*.

Ko, J., Ko, S., Son, H., Yoo, B., Cheon, J. and Kim, H. (2015a). Development of brake system and regenerative braking co-operative control algorithm for automatic transmission-based hybrid electric vehicle. *IEEE Trans. Vehicular Technology* **64**, **2**, 431–440.

Ko, J., Lee, G., Ko, S., Ahn, S., Kim, H., Choi, S., Kim, I., Jeong, J., Hyun, D. and Kim, H. (2012). Co-operative control of regenerative braking using a front electronic wedge brake and a rear electronic mechanical brake considering the road friction characteristic. *SAE Paper No*. 2012-01-1798.

Ko, S., Ko, J., Lee, S., Cheon, J. and Kim, H. (2013a). A study on in-wheel motor control to improve vehicle stability using human-in-the-loop simulation. *J. Power Electronics* **13**, **4**, 536–545.

Ko, S., Ko, J., Lee, S., Cheon, J. and Kim, H. (2015b). A study on road friction coefficient estimation and motor torque control for an in-wheel electric. *Proc. Inst. of Mech. Eng. Part D: J. Automobile Engineering* **229**, **5**, 611–623.

Ko, S., Song, C., Park, J., Ko, J., Yang, I. and Kim, H. (2013b). Comparison of braking performance by electro-hydraulic ABS and motor torque control for in-wheel electric vehicle, *EVS27*, 1–6.

Lee, J., Jung, S., Heo, S., Choi, H., Kim, H., Noh, K., Park, I. and Kim, J. (2010). Improvement of road friction estimation using full vehicle model. *Spring Conf. Proc*., *Korean Society of Automotive Engineers*, 168–171.

Limpert, R. (1992). Brake Design and Safety. SAE

International, Warrendale, Pennsylvania. Chapter 7.

Liu, X., Li, L., Hori., Y., Akiba, T. and Shirato, R. (2005). Optimal traction control for EV utilizing fast torque response of electric motor. *IECON 2005 31st Annual Conf., IEEE*, 2614–2619.

Nakao, Y., Kawasaki, H. and Major, D. (2002). Estimation of friction levels between tire and road. *SAE World Cong.,* Detroit, USA.

Nam, K., Fujimoto, H. and Hori, Y. (2012). Lateral stability control of in-wheel-motor-driven electric vehicles based on sideslip angle estimation using lateral tire force sensors. *IEEE Trans. Vehicular Technology* **61**, **5**, 1972–1985.

Park, M., Kim, S., Yang, L. and Kim, K. (2009). Development of the control logic electronically controlled hydraulic brake system for hybrid vehicle. *SAE Paper No*. 2009-01-1215.

Rajamani, R., Phanomchoeng, G., Piyabongkarn, D. and Lew, J. (2012). Algorithms for real-time esimation of individual wheel tire-road friction coefficients. *IEEE Trans. Mechatronics* **17**, **6**, 1183–1195.

Rajamani, R., Piyabongkarn, D., Lew, J., Yi, K. and Phanomchoeng, G. (2010). Tire-road frcition-coefficient estimation. *Control System, IEEE* **30**, **4**, 54–69.

Sakai, S., Sado, H. and Hori, Y. (1999). Motion control in an electric vehicle with 4-independently driven in-wheel motors. *IEEE/ASME Trans. Mechatronics* **4**, **1**, 9–16.

Soga, M., Shimada, M., Sakamoto, J. and Otomo, A. (2002). Development of vehicle dynamics management system for hybrid vehicle: ECB system for improved environmental and vehicle dynamic performance. *JSAE Rev.* **23**, **4**, 459–464.

Walker, A., Lamperth, M. and Wilkins, S. (2002). On friction braking demand with regenerative braking. *SAE Paper No*. 2002-01-2581.

Wang, J., Alexander, L. and Rajamani, R. (2004). Friction estimation on highway vehicles using longitudinal measurements. *J. Dynamic, Measurement, and Control* **126**, **2**, 265–275.

Yeo, H., Koo, C., Jung, W., Kim, D. and Cheon, J. (2011). Development of Smart Booster Brake System for Regenerative Brake Cooperative Control. *SAE Paper No*. 2011-01-2356.